https://doi.org/10.1016/j.applthermaleng.2017.03.027

The thermal effect in Direct Carbon Solid Oxide Fuel Cells

Haoran Xu[1], Bin Chen[1], Houcheng Zhang[1,2], Wei Kong[1,3], Bo Liang[4], Meng Ni[1,*]

[1] Building Energy Research Group, Department of Building and Real Estate
The Hong Kong Polytechnic University, Hung Hom, Kowloon, Hong Kong, China
[2] Department of Microelectronic Science and Engineering, Ningbo University, Ningbo 315211, China
[3]School of Energy and Power Engineering, Jiangsu University of Science and Technology, Zhenjiang, 212003, China
[4] School of Materials and Energy, Guangdong University of Technology, Guangzhou, 510006, China

Abstract:

In this paper, a numerical model is developed to investigate the influence of operating parameters on the temperature field distribution and the performance of a tubular direct carbon solid oxide fuel cell (DC-SOFC). The model is validated by comparing the simulation results with experimental data from the literature. Parametric simulations are conducted to investigate the effects of various operating and structural parameters on the thermal behaviors of DC-SOFCs. It is found that the operating parameters greatly influences the DC-SOFC thermal behaviors and the temperature field in DC-SOFC is highly non-uniform. The position of peak temperature in the cell is highly dependent on the operating potential. In addition, it is found that a smaller distance between the carbon bed and the anode electrode is beneficial for improving the temperature uniformity in the DC-SOFC. The breakdown of heat generation/consumption in DC-SOFC shows that the anode processes contribute the most to the temperature variation in the cell. The results of the present study form a solid foundation for better thermal management of DC-SOFC.

Keywords: Solid oxide fuel cell (SOFC); Carbon; Temperature; Mathematical modeling

* Corresponding author:
Email: bsmengni@polyu.edu.hk; Tel: 852-27664152; Fax: 852-27645131.

1. Introduction

Solid carbon is the major component of fossil fuels. It can also be obtained easily from cheap and renewable biomasses such as waste wood and leaves. Solid carbon fuels are usually used in conventional thermal power plants which will produce significant amount of pollutants and hazardous gases such as CO_2, SO_x and NO_x as byproduct [1, 2]. In addition, the efficiency of power generation by thermal power plant is typically below 40% or even about 30% if carbon capture and storage is adopted to reduce the pollutant emission [3]. Therefore, more efficient and environmental friendly strategy using solid carbon fuel for power generation is of practical importance since carbon-based fuel will continue to be the major energy source for a long time.

Solid oxide fuel cell (SOFC) is an advanced energy conversion device which converts the chemical energy in the fuel into electrical energy through electrochemical reaction with a high efficiency (50-60%) [4, 5]. An SOFC has an all solid-state structure with a dense electrolyte sandwiched between two porous electrodes. In SOFCs, the fuel and oxidant are separated by the oxygen-ion-conducting electrolyte, resulting in easy emission control. The high operating temperature of SOFCs (about 800^{o}C) facilitates the electrochemical reaction kinetics, thus low cost catalyst such as Ni can be used. In addition, SOFCs can use not only H_2, but also other various fuels like hydrocarbon fuels, solid carbon, and ammonia for power generation [6, 7].

The direct use of solid carbon as a fuel in SOFCs offers a new strategy for efficient and environmental friendly power generation. Due to its high efficiency and easy emission control, the direct-carbon solid oxide fuel cell (DC-SOFC) has received more and more attention in recent years. Li et al. [8] combined fluidized bed and DC-SOFC to convert solid carbon into electricity for the first time. Based on GC analysis of the reaction products, it was

proposed that the intermediate species CO was electrochemically oxidized at the anode electrode. Andrew et al. [9] performed system exergy analyses of DC-SOFCs and found that the conversion efficiency of DC-SOFCs was much higher than a carbon fueled SOFC system with separate carbon gasification unit and SOFC unit. They also demonstrated a power density of 220 mW cm^{-2} at 0.68 V at 1178 K. Wu et al.[10] adopted Fe_mO_n-M_xO (M = Li, K, Ca) as catalyst to enhance the Boudouard reaction in SOFC anode and achieved a peak power density of about 297 mW cm^{-2} at 1123 K. Li et al.[11] also found that by introducing appropriate catalyst into DC-SOFC, the operating temperature can be decreased. Bai et al.[12] assembled and tested a 3-cell-stack DC-SOFC and achieved a peak power density of 465 mW cm^{-2} at 1123 K. They also found that larger current resulted in shorter life time and smaller carbon fuel utilization in the single cells. Alexander et al. [13, 14] proposed a steam-carbon-air fuel cell for H_2 and electricity co-generation. A high efficiency of above 78% was achieved for H_2 and electricity co-generation. Gur et al. [8] proposed the CO2 shuttling mechanisms in DC-SOFC : the electrochemically produced CO_2 from CO at the triple phase boundary (TPB) of SOFC diffuses to the C bed for CO production from C by Boudouard reaction. Xie et al. [1, 15] experimentally verified the reaction mechanism of DC-SOFCs by comparing the performance of a DC-SOFC with an SOFC operating on pure CO. They also proposed CO gas and electricity co-generation through a DC-SOFC. It was found that the overall efficiency for gas-electricity co-generation was almost twice of the electrical conversion efficiency. Zhou et al.[16] fabricated a cathode supported tubular DC-SOFC with a continuous fuel supply to the anode. They proposed that the distance between carbon fuel and anode electrode could affect the performance of the cell, which was verified by Xu et al.[17] through their modeling work.

Jiao et al.[18] used structurally modified coal char as fuel in a DC-SOFC and found that the Boudouard reaction activity was greatly improved, which consequently improved the power output of the cell.

The above-mentioned studies demonstrated great potential of DC-SOFC and attempted to understand the fundamental mechanisms in DC-SOFC. However, to the best knowledge of authors, there is no detailed thermal analysis of DC-SOFCs in the current literatures. Considering that the temperature distribution in DC-SOFCs not only affects the chemical reaction and electrochemical reaction of the cells, but also affects the life time of DC-SOFCs due to the heat management and thermal stress. In this paper, the previously developed model is extended to study the thermal effects on the DC-SOFC temperature distribution which is the new contribution of this paper.

2. Model development

2.1. Model assumption and calculation domain

A 2D numerical model including the electrochemical and chemical reactions, ionic/electronic charge transport, mass/momentum transport and heat transfer is developed for a tubular direct carbon solid oxide fuel cell. This model is an extension from our previous work[17] which has been well validated. Compared with our previous work, cell length in this model has been extended from 9mm to 90mm, and thermal effect has also been considered to investigate the cell temperature distribution.

The schematic of the electrolyte supported tubular DC-SOFC is shown in Fig. 1(a). Carbon fuel is supplied to the anode chamber and air is supplied to the cathode channel. Initial

CO/CO_2 comes from the reactions between carbon fuel and initial O_2 in the anode chamber. CO molecules produced in anode chamber diffuse into the porous anode electrode and react with O^{2-} through electrochemical reaction at TPB sites where CO_2 molecules are then formed and electrons are released. After that, the produced CO_2 molecules in anode electrode diffuse back to the chamber and react with solid carbon to produce more CO molecules through Boudouard reaction. These processes repeat continuously between the anode chamber and the anode electrode to maintain CO/CO_2 cycling while generating electricity, related formulas are shown in Eqs. (1-5).

The main assumptions in this model are shown as below.

(1) The electrochemical reactions take place on triple phase boundaries (TPBs), which are assumed to be uniformly distributed in the whole porous electrodes. The two conducting phases (electronic and ionic) in the porous electrodes are continuous and homogeneous.

(2) The ionic and electronic charge transport processes take place in the Positive Electrode-Electrolyte-Negative electrode (PEN) assembly.

(3) All gases (CO, CO_2, O_2 and N_2) are ideal gases. The gas flow is incompressible.

(4) The volume of activated carbon fuel in the anode chamber does not change in the steady state model.

(5) Thermal radiation is assumed to be negligible.

2.2. Governing equations

This 2D numerical model fully considers the electrochemical and chemical reactions, ionic/electronic charge transport, mass/momentum transport and heat transfer processes. The 2D model consists of the following sub-models: chemical reaction model, electrochemical reaction model, mass transport model, fluid flow model and heat transfer model.

2.2.1. Chemical reaction model

Unlike gas fuel fed solid oxide fuel cells, the fuel for DC-SOFCs is solid carbon. Although CO is the real material that participates in electrochemical reaction which happens in anode electrode. It is solid carbon that offers chemical energy, and CO is the intermediate that transports chemical energy from solid carbon to anode electrode. Thus the chemical reaction (Boudouard reaction) is a key process in this system. The Boudouard reaction is described as shown in reaction (1)

$$C + CO_2 \leftrightarrow 2CO \tag{1}$$

The reaction rate of Boudouard reaction (R_{rb}) are calculated as shown in Eq. (2) [19]:

$$R_{rb} = k_{rb} \exp\left(-E_{rb}/RT\right) c_{CO_2} \tag{2}$$

2.2.2. Electrochemical reaction model

The electrochemical reaction model is developed to calculate the electrochemical reaction rate at given operating conditions. As shown in Fig. 1(a), the gas mixture of CO/CO_2 flows in the anode while air is supplied to the cathode. O_2 molecules diffuse from cathode channel into the TPB sites in porous cathode electrode, where they are reduced to form oxygen ions (O^{2-}) via reactions (3).

$$O_2 + 4e^- \rightarrow 2O^{2-} \quad (3)$$

The oxygen ions transport through the dense electrolyte to TPB sites in the anode, where they electrochemically react with CO molecules to form CO_2 and release electrons as shown in reaction (4):

$$2CO + 2O^{2-} \rightarrow 2CO_2 + 4e^- \quad (4)$$

As CO is the actual material that participate in the electrochemical reaction instead of solid carbon in DC-SOFC. The overall electrochemical reaction can be obtained by combining reaction (3) and reaction (4) as shown in reaction (5):

$$2CO + O_2 \rightarrow 2CO_2 \quad (5)$$

Related operating potential can be determined by its thermodynamic equilibrium potential and operating overpotential losses as shown in Eq. (6):

$$V = E_{eq} - \eta_{act,an} - \eta_{act,ca} - \eta_{ohmic} \quad (6)$$

Here E_{eq} is the equilibrium potential (Nernst potential) of the overall electrochemical reaction which is determined by the thermodynamic property of the reaction. η_{act} is the activation overpotential which reflects the energy barrier needed to overcome for the electrochemical reaction to proceed. η_{ohmic} is the ohmic overpotential from the ionic/electronic conduction. The concentration overpotentials are not considered in Eq. (6) as local gas partial pressures at the TPB are used in the equilibrium potential calculation.

2.2.2.1. Equilibrium potential

As CO participates in the electrochemical reaction in DC-SOFCs, the related equilibrium

potential for reaction (5) can be calculated by Eq. (7):

$$E_{CO} = E_{CO}^{0} + \frac{RT}{2F}\ln\left[\frac{P_{CO}^{L}(P_{O_2}^{L})^{1/2}}{P_{CO_2}^{L}}\right] \quad (7)$$

Here E^0 is the potential under standard conditions, R is the universal gas constant (8.3145 J mol^{-1} K^{-1}), T is the operating temperature (K), F is the Faraday constant (96485 C mol^{-1}). P_{CO}^{L}, $P_{CO_2}^{L}$ and $P_{O_2}^{L}$ are the local partial pressures of CO, CO_2 and O_2, respectively. The value of E_{CO}^{0} can be calculated by Eq. (8)[20]:

$$E_{CO}^{0} = 1.46713 - 0.0004527T \quad (8)$$

Thus, the Nernst potential can be calculated as shown in Eq. (9) by combining Eq. (7) and Eq. (8).

$$E_{co} = 1.46713 - 0.0004527T + \frac{RT}{2F}\ln\left[\frac{P_{CO}^{L}(P_{O_2}^{L})^{1/2}}{P_{CO_2}^{L}}\right] \quad (9)$$

2.2.2.2. Activation overpotential

Activation overpotential is the potential loss involved in the electrochemical reaction, which is related with the electrochemical reaction kinetics. Butler-Volmer equation is adopted to describe the relationship between the activation overpotential and the current density [21].

$$i = i_0\left\{\exp\left(\frac{\alpha n F \eta_{act}}{RT}\right) - \exp\left(\frac{(1-\alpha) n F \eta_{act}}{RT}\right)\right\} \quad (10)$$

Here i_0 is the exchange current density representing the activity of the electrochemical reaction, α is the electronic transfer coefficient and n is the number of electrons transferred in a single electrochemical reaction.

2.2.2.3. Ohmic overpotential

The ohmic overpotential in the DC-SOFC results from ion/electron conduction, thus it is largely dependent on the ionic/electronic conductivity of electrode and electrolyte. The ohmic overpotential can be calculated with the Ohm's law as shown in Eq. (11) and Eq. (12):

$$i_l = -{\sigma_l}^{eff} \nabla(\emptyset_l) \tag{11}$$

$$i_s = -\sigma_{s.eff} \nabla(\emptyset_s) \tag{12}$$

Here $\sigma_{l.eff}$ and $\sigma_{s.eff}$ are the effective ionic and electronic conductivities, respectively. $\emptyset_l$ and $\emptyset_s$ are the ion conducting and electron conducting electric potentials, respectively. In the porous electrodes, the effective conductivities are related to the structural parameters including volume fraction and tortuosity as shown in Eq. (13) and Eq. (14).

$${\sigma_l}^{eff} = \sigma_l \cdot \frac{V_l}{\tau_l} \tag{13}$$

$${\sigma_s}^{eff} = \sigma_s \cdot \frac{V_s}{\tau_s} \tag{14}$$

Here σ_l and σ_s are the intrinsic ionic and electronic conductivities, V_l and V_s are the volume fraction value in ionic and electronic phases, τ_l and τ_s are the tortuosity value in ionic and electronic phases.

2.2.3. Mass transport model

In the gas channel and porous electrodes, both free molecular diffusion and Knudsen diffusion are considered in this mass transport model. Free molecular diffusion dominates in gas channel and large pores while Knudsen diffusion becomes significant when pore sizes are

comparable or smaller than molecular mean-free path. The extended Fick's model is used to describe gas transport in the channel and porous electrodes as shown in Eq. (15):

$$N_i = -\frac{1}{RT}\left(\frac{B_0 y_i P}{\mu}\frac{\partial \mathrm{P}}{\partial \mathrm{z}} - D_i^{eff}\frac{\partial (y_i \mathrm{P})}{\partial \mathrm{z}}\right) \ (i = 1, \dots, n) \tag{15}$$

Where N_i represents the flux of mass transport, B_0 is the permeability coefficient, y_i is the mole fraction of component i, μ is the dynamic viscosity of the gas mixture and D_i^{eff} is the effective diffusivity of species *i*. The effective diffusion coefficient (D_i^{eff}) considering both molecular diffusion coefficient (D_{im}^{eff}) and Knudsen diffusion coefficient (D_{ik}^{eff}) and can be calculate as Eq. (16):

$$D_i^{eff} = \frac{\varepsilon}{\tau}\left(\frac{1}{D_{im}^{eff}} + \frac{1}{D_{ik}^{eff}}\right)^{-1} \tag{16}$$

Here ε is the volume fraction of the pores, τ is the tortuosity factor. D_{im}^{eff} and D_{ik}^{eff} depend on the micro-structure of the porous electrode and operating conditions. More detailed calculation procedures of these two parameters can be found in reference [22-24].

2.2.4. Fluid flow model

The general Navier-Stokes (N-S) equation is used to describe the momentum conservation. For momentum conservation in channels, the N-S equation can be described as shown in Eq. (17):

$$\rho\frac{\partial u}{\partial t} + \rho u \nabla u = -\nabla p + \nabla\left[\mu\left(\nabla u + (\nabla u)^T\right) - \frac{2}{3}\mu\nabla u\right] \tag{17}$$

For momentum conservation in porous electrodes and the anode chamber, the N-S equation is modified by including the Darcy's term for momentum conservation:

$$\rho\frac{\partial u}{\partial t}+\rho u\nabla u=-\nabla p+\nabla[\mu\left(\nabla u+(\nabla u)^{T}\right)-\frac{2}{3}\mu\nabla u\Big]-\frac{\varepsilon\mu u}{k} \quad (18)$$

Here ρ is the gas density, u is the velocity vector, p is pressure and ε is the porosity of the electrode.

2.2.5. Heat transfer model

In DC-SOFCs, electrochemical reactions in TPB sites generates heat while the chemical reaction (Boudouard reaction) in anode chamber consumes heat. This will not only result in the gradient of temperature along the cell length, but also along the cell width. General heat balance equation is used to describe the heat transfer in the cell as:

$$\rho C_p u\cdot\nabla T+\nabla\cdot\left(-\lambda_{eff}\nabla T\right)=Q \quad (19)$$

where C_p is the fluid heat capacity at constant pressure, u is the fluid velocity field, λ_{eff} is the effective thermal conductivity and Q is the heat source. In the porous structure of electrodes, λ_{eff} can be calculated as:

$$\lambda_{eff}=(1-\varepsilon)\lambda_s+\varepsilon\lambda_l \quad (20)$$

where λ_s and λ_l are heat conductivity of solid and liquid phase, respectively. Value of above material property parameters are listed in Table 1.

2.3. Boundary conditions

2.3.1. Electrochemical reaction

The electric potentials are specified at the outer boundaries of cathode and anode as working

potential and zero potential, respectively. The insulation condition is applied to the bottom and top of the cell.

2.3.2. Mass transport

Inflow gas mole fraction is specified at the inlet of the cathode. The convective flux boundary condition is specified at the outlets of the cathode and anode. Zero flux is assumed at the end of anode chamber, electrolyte/electrode interface and the ends of electrodes.

2.3.4. Fluid flow

Standard gas flow rate (standard cubic centime per minute: SCCM) is specified at the cathode while pressure condition is specified at the outlet. No-slip condition is applied to the end of anode chamber, electrolyte/electrode interface and the ends of electrodes.

2.3.5. Heat transfer

Thermal insulation condition is applied to the outer boundary of cathode chamber, the end of anode chamber and the ends of electrodes and electrolyte. Gas temperature is specified at the cathode inlet.

2.4. Model parameters

The values of material thermal properties and tuning parameters are summarized in Table 1 and Table 2, more detailed information can be found in our previous work[17]. In the parametric simulations, the parameters are varied to evaluate their effects on the DC-SOFC performance, detailed operating parameters are listed in Table 3 to Table 5.

2.5. Model solution

The model is solved at certain cell potential, inlet gas flow rate and inlet gas temperature. The output of the model is mainly the temperature distribution. The calculations are performed using the finite element commercial software COMSOL MULTIPHSICS®.

2.6 Model validation

This model is an extension of our previous model, which has already been validated by comparing the simulation results and experimental data from the literature as shown in Fig. 1(b). More detailed information about the model validation can be found in [17].

3. Results and discussion

3.1. Effect of applied voltage

The relationship between operating potential, current density and average electrolyte temperature at given operating conditions are shown in Fig. 2. The detailed operating conditions are listed in Table 3.

As can be seen in Fig. 2, when operating potential decreases from 1.0 V to 0.6 V, the cell current density increases from 754 A m^{-2} to 5417 A m^{-2}. The average electrolyte temperature decreases slightly when the operating potential decreases from 1035 K at 1.0 V to 1029 K at 0.9 V and increases quickly to 1104 K at 0.6 V. The electrochemical reaction rate and overpotential losses are higher at a lower operating potential, leading to more heat generation.

However, more CO_2 can be generated at a higher current density, which in turn leads to a higher rate of the endothermic Boudouard reaction and more heat consumption in the anode chamber. These combined effects result in the slightly temperature decrease when operating potential decreases from 1.0 V to 0.9 V. With a further decrease of operating potential from 0.9 V to 0.6 V, the temperature of DC-SOFC is increased substantially, indicating that the heat generation from the electrochemical reactions and overpotential losses is higher than heat consumption by Boudouard reaction.

The temperature distribution of the DC-SOFC is shown in Fig. 3. At an operating potential of 1.0 V, the temperature decreases along the DC-SOFC length and the peak temperature occurs at the cathode inlet. While at an operating potential of 0.6 V, the temperature increases along the cell length and the peak temperature occurs at the cathode outlet. The different temperature distribution patterns are caused by the electrochemical and chemical processes in the DC-SOFC. At a high operating potential, the heat generation from electrochemical reaction and overpotential losses is lower than heat consumption by endothermic Boudouard reaction, leading to a decrease of cell temperature. While at a relatively lower operating potential, exothermic processes are greatly enhanced due to increased current density, which in turn increase the temperature of DC-SOFC.

The temperature of the anode temperature is found to be always lower than the cathode temperature at the same cell length position, as endothermic Boudouard reaction takes place in the anode chamber. It is important to point out that the temperature distribution of the DC-SOFC is almost uniform at an operating potential of about 0.65V. For long-term and stable operation DC-SOFC, the uniform temperature distribution is desirable to reduce the thermal

stress in the cell. The results of the present study clearly demonstrate that the temperature uniformity of DC-SOFC can be achieved by controlling the operating conditions.

Fig. 4. shows a breakdown on heat generation/consumption from different components in the cell. It can be seen that the porous anode and the anode chamber contribute most to the heat generation and consumption, respectively. At an operating potential of 1.0 V, the heat consumption by Boudouard reaction in the anode chamber is slightly higher than the heat generation from electrochemical reaction and overpotential losses, which well explains the thermal effect in Figure 3. In the porous anode, the entropy change due to electrochemical reaction contributes to over 90% of heat generation in the anode while activation loss in anode contributes to about 9.85%. At an operating potential of 0.6, both the heat generation and heat consumption are substantially enhanced and the heat generation from electrolyte and the cathode are not negligible. The total heat generation is found to be higher than the heat consumption, again in consistence with the results in Figure 3. Compared with the 1V case, the anode activation loss contributes to about 29% of the total heat generation in the anode at 0.6V. The results suggest that the heat generation/consumption in the anode is the key for controlling the temperature field of DC-SOFC. Thus it is possible to adjust the operating parameters to control the chemical and electrochemical processes in the anode to control the temperature distribution in DC-SOFC.

3.2. Effect of cathode inlet gas temperature

Inlet gas temperature will also affect the temperature distribution in the cell. Detailed operating parameters are listed in Table 4.

As shown in Fig. 5, at a potential of 1 V, cell temperature decreases from inlet to outlet along the cell length at cathode inlet gas temperature from 1023K to 1173K. It can also be found from Fig. 5 that the temperature gradient along the cell length increases with increasing cathode inlet gas temperature. As shown in Fig. 6(a), when the operating potential is 0.6V, cell temperature increases from inlet to outlet along the cell length. However, it should also be noted that when cell operates with a relative high cathode inlet gas temperature (1123 K), the peak temperature could occur at the middle of the DC-SOFC. This is because electrochemical reaction rate is very high at a high temperature and low operating potential and oxygen is almost exhausted in the cathode channel (Fig. 6(b)), resulting in nearly zero electrochemical reaction and no heat generation in the end of the DC-SOFC. For comparison, the rate of endothermic chemical reaction is still high throughout the anode chamber, decreasing the temperature of DC-SOFC in the downstream.

3.3. Effect of distance between carbon and anode electrode

Previous study has shown how the distance between carbon fuel and anode electrode (Dce) will affect the performance of DC-SOFC [17]. As the thermal conductivity of gas is much smaller than that of solid carbon, the increase of Dce will surely increase the variation of temperature in the cell. Thus the effect of Dce on the temperature distribution of the cell is discussed, detailed operating parameters are listed in Table 5.

Fig. 7 shows the effects of Dce on the temperature distribution in the cell with 1073K cathode inlet gas temperature and 0.7 V operating potential. Distance between carbon and anode

electrode surface varies from 59 μm to 2059 μm in this study. As can be seen from Fig. 7, when Dce is quite small (59 μm), the gradient along the cell width is quite small. With the increase of Dce, there occurs an obvious temperature boundary between solid carbon and anode gas channel and the gradient along the cell width becomes quite large.

Besides, it is observed from Fig. 8 that the CO molar fraction in anode decreases quickly with the increase of Dce, which is due to the increased gas transport difficulty and lower chemical reaction temperature caused by larger Dce. Thus, it is also important to keep a small distance between carbon fuel and anode electrode when cell is placed horizontally.

4 Conclusions

A multi-physics model considering electrochemical reaction, chemical reactions, ionic/electronic charge transport, mass/momentum transport and heat transfer is developed to characterize the temperature distribution of a tubular DC-SOFC. Parametric simulations are conducted to evaluate the effects of operating potential, cathode inlet gas temperature and distance between the carbon fuel and anode electrode on DC-SOFC temperature distribution.

It is found that the operating potential has a great effect on the temperature distribution of the cell. With the decrease of operating potential, the overall cell temperature increases quickly. Beside, the temperature gradient also changes from negative to positive along the cell length with the cell operating potential decreasing from 1.0 V to 0.6 V and a relative even temperature distribution of the cell is found when the operating potential is around 0.65V. It is also observed from the breakdown analysis that most of the heat is generated from anode electrode, where

entropy change heat is the majority part compared with other processes.

Cathode inlet gas temperature is also found to play an important role on the temperature distribution of the cell. When the operating voltage is high (1.0 V), cathode inlet gas plays as the outer heat source and it plays as the outer heat sink when the operating voltage is low (0.6 V). It should also be noted that when the cathode inlet gas temperature is high (1123K), cathode oxygen may be exhausted in the cell, which not only causes a peak temperature point in the middle position of the cell length but also decreases cell's electrochemical performance.

The effect of distance between carbon fuel and anode electrode on temperature distribution is also studied in this work. It is found that the temperature gradient increases quickly along the cell width with the increase of Dce due to the small thermal conductivity of the gas.

Acknowledgement

This research is supported by a grant of SFC/RGC Joint Research Scheme (X-PolyU/501/14) from Research Grant Council, University Grants Committee, Hong Kong SAR.

We gratefully acknowledge the financial support of the National Science Foundation of China (Grant No. 51406091 and Grant No. 21406095).

Nomenclature

Abbreviation

DC-SOFC	Solid oxide fuel cell direct using carbon as fuel
PEN	Positive Electrode-Electrolyte-Negative electrode assembly
SCCM	Standard cubic centime per minute
SOFC	Solid oxide fuel cell
TPB	Triple phase boundary

Roman

B_0	Permeability coefficient, m^2
c_{CO_2}	Molar concentration of carbon dioxide, $mol \cdot m^{-3}$
C_p	Heat capacity, $J \cdot K^{-1}$
D_{ce}	Distance between carbon and anode electrode
D_i^{eff}	Effective diffusivity of species i, $m^2 \cdot s^{-1}$
D_{ik}^{eff}	Knudsen diffusion coefficient of i, $m^2 \cdot s^{-1}$
D_{im}^{eff}	Molecular diffusion coefficient of i, $m^2 \cdot s^{-1}$
E_a	Active energy, $J \cdot mol^{-1}$
E_{CO}	Equilibrium potential for carbon monoxide oxidization, V
E_{CO}^0	Standard equilibrium potential for carbon monoxide oxidization, V
E_{eq}	Equilibrium Nernst potential, V
E_{rb}	Active energy of Boudouard reaction, $J \cdot mol^{-1}$
F	Faraday constant, 96485 $C \cdot mol^{-1}$
i_o	Exchange current density, $A \cdot m^{-2}$
k_{rb}	Equilibrium constant of Boudouard reaction, s^{-1}
L_{cell}	Length of the cell, mm
n	Number of electrons transferred per electrochemical reaction
N_i	Flux of mass transport, $kg \cdot m^{-3} \cdot s^{-1}$
p	(partial) Pressure, Pa
R	Gas constant, 8.314 $J \cdot mol^{-1} \cdot K^{-1}$
R_{ce}	Ratio D_{ce} and cell length
R_{ce}	Reaction rate of Boudouard reaction, $mol \cdot m^{-3} \cdot s^{-1}$
T	Temperature, K
u	Velocity field, $m^3 \cdot s^{-1}$
V	Volume fraction
y_i	Molar fraction of component i

Greek letters

α	Charge transfer coefficient
β_{H_2}	Electrochemical kinetics parameter for H_2
ε	Porosity
$\eta_{act,an}$	Anode activation polarization, V
$\eta_{act,ca}$	Cathode activation polarization, V
η_{ohmic}	Ohmic polarization, V
κ	Permeability, m^2
λ	Thermal conductivity, $W \cdot m^{-1} K^{-1}$
μ	Dynamic viscosity of fluid, Pa·s
ρ	Fluid density, $kg \cdot m^{-3}$

σ	Conductivity, S/m
τ	Tortuosity
∅	Potential, V

Subscripts	
an	Anode
ca	Cathode
co	Carbon monoxide
l	Ionic phase
s	Electronic phase

Superscripts	
0	Parameter at equilibrium conditions
eff	Effective
L	Local

References

[1] Xie Y, Cai W, Xiao J, Tang Y, Liu J, Liu M. Electrochemical gas-electricity cogeneration through direct carbon solid oxide fuel cells. J Power Sources. 2015;277:1-8.

[2] Liu R, Zhao C, Li J, Zeng F, Wang S, Wen T, et al. A novel direct carbon fuel cell by approach of tubular solid oxide fuel cells. J Power Sources. 2010;195:480-2.

[3] Giddey S, Badwal SPS, Kulkarni A, Munnings C. A comprehensive review of direct carbon fuel cell technology. Progress in Energy and Combustion Science. 2012;38:360-99.

[4] Ni M. Modeling and parametric simulations of solid oxide fuel cells with methane carbon dioxide reforming. Energ Convers Manage. 2013;70:116-29.

[5] Zhang H, Chen J, Zhang J. Performance analysis and parametric study of a solid oxide fuel cell fueled by carbon monoxide. Int J Hydrogen Energ. 2013;38:16354-64.

[6] Ni M. Thermo-electrochemical modeling of ammonia-fueled solid oxide fuel cells considering ammonia thermal decomposition in the anode. Int J Hydrogen Energ. 2011;36:3153-66.

[7] Ni M, Leung DYC, Leung MKH. Thermodynamic analysis of ammonia fed solid oxide fuel cells: Comparison between proton-conducting electrolyte and oxygen ion-conducting electrolyte. J Power Sources. 2008;183:682-6.

[8] Li S, Lee AC, Mitchell RE, Gür TM. Direct carbon conversion in a helium fluidized bed fuel cell. Solid State Ionics. 2008;179:1549-52.

[9] Lee AC, Mitchell RE, Gür TM. Thermodynamic analysis of gasification-driven direct carbon fuel cells. J Power Sources. 2009;194:774-85.

[10] Wu Y, Su C, Zhang C, Ran R, Shao Z. A new carbon fuel cell with high power output by integrating with in situ catalytic reverse Boudouard reaction. Electrochemistry Communications. 2009;11:1265-8.

[11] Li C, Shi Y, Cai N. Performance improvement of direct carbon fuel cell by introducing catalytic gasification

process. J Power Sources. 2010;195:4660-6.
[12] Bai Y, Liu Y, Tang Y, Xie Y, Liu J. Direct carbon solid oxide Fuel Cell—a potential high performance battery. Int J Hydrogen Energ. 2011;36:9189-94.
[13] Alexander BR, Mitchell RE, Gür TM. Steam-Carbon Fuel Cell Concept for Cogeneration of Hydrogen and Electrical Power. J Electrochem Soc. 2011;158:B505-B13.
[14] Alexander BR, Mitchell RE, Gür TM. Viability of Coupled Steam-Carbon-Air Fuel Cell Concept for Spontaneous Co-Production of Hydrogen and Electrical Power. J Electrochem Soc. 2012;159:F810-F8.
[15] Xie Y, Tang Y, Liu J. A verification of the reaction mechanism of direct carbon solid oxide fuel cells. Journal of Solid State Electrochemistry. 2012;17:121-7.
[16] Zhou J, Ye XF, Shao L, Zhang XP, Qian JQ, Wang SR. A promising direct carbon fuel cell based on the cathode-supported tubular solid oxide fuel cell technology. Electrochimica Acta. 2012;74:267-70.
[17] Xu H, Chen B, Liu J, Ni M. Modeling of direct carbon solid oxide fuel cell for CO and electricity cogeneration. Applied Energy. 2016;178:353-62.
[18] Jiao Y, Zhao J, An W, Zhang L, Sha Y, Yang G, et al. Structurally modified coal char as a fuel for solid oxide-based carbon fuel cells with improved performance. J Power Sources. 2015;288:106-14.
[19] Mon E, Amundson NR. Diffusion and Reaction in a Stagnant Boundary Layer about a Carbon Particle. 2. An Extension. Industrial & Engineering Chemistry Fundamentals. 1978;17:313-21.
[20] Ni M. Modeling of SOFC running on partially pre-reformed gas mixture. Int J Hydrogen Energ. 2012;37:1731-45.
[21] Kakaç S, Pramuanjaroenkij A, Zhou XY. A review of numerical modeling of solid oxide fuel cells. Int J Hydrogen Energ. 2007;32:761-86.
[22] Suwanwarangkul R, Croiset E, Fowler MW, Douglas PL, Entchev E, Douglas MA. Performance comparison of Fick's, dusty-gas and Stefan–Maxwell models to predict the concentration overpotential of a SOFC anode. J Power Sources. 2003;122:9-18.
[23] Todd B, Young JB. Thermodynamic and transport properties of gases for use in solid oxide fuel cell modelling. J Power Sources. 2002;110:186-200.
[24] Chan SH, Khor KA, Xia ZT. A complete polarization model of a solid oxide fuel cell and its sensitivity to the change of cell component thickness. J Power Sources. 2001;93:130-40.
[25] Ni M. 2D heat and mass transfer modeling of methane steam reforming for hydrogen production in a compact reformer. Energ Convers Manage. 2013;65:155-63.
[26] Luo Y, Shi Y, Li W, Cai N. Comprehensive modeling of tubular solid oxide electrolysis cell for co-electrolysis of steam and carbon dioxide. Energy. 2014;70:420-34.

List of Tables

Table.1 Material thermodynamic properties[25, 26]

Parameters	**Value**	**Unit**
Thermal conductivity		
Carbon	1.59	$W\ m^{-1}K^{-1}$
Electrode	13.54	$W\ m^{-1}K^{-1}$
Electrolyte	2.7	$W\ m^{-1}K^{-1}$
Specific heat capacity		
Carbon	887.5	$J\ kg^{-1}K^{-1}$
Electrode	390	$J\ kg^{-1}K^{-1}$
Electrolyte	300	$J\ kg^{-1}K^{-1}$
Density		
Carbon	1700	$kg\ m^{-3}$
Electrode	6870	$kg\ m^{-3}$
Electrolyte	2000	$kg\ m^{-3}$

Table. 2 Model tuning parameters

Parameter	**Value**	**Unit**
Cathode tortuosity	3	
Anode tortuosity	3	
O_2 exchange current density i_{O_2}	400	Am^{-2}
CO exchange current density, i_{CO}	450	Am^{-2}
CO charge transfer coefficient, α_{CO}	0.5	
O_2 charge transfer coefficient, α_{O_2}	0.5	
Equilibrium constant of Boudouard reaction	$6 \times 10^{13} \cdot \frac{T-973}{150}$	1/s

Table. 3 Operation parameters for operating potential effect study in DC-SOFC

Parameter	**Value**	**Unit**
Operating potential	0.6 – 1.0	V
Anode inlet gas flow rate	0	
Cathode inlet gas flow rate	400	SCCM
Cathode gas composition	Air	
Cathode inlet gas temperature	1073	K

Table. 4 Operation parameters for cathode inlet gas temperature effect study in DC-SOFC

Parameter	**Value**	**Unit**
Operating potential	0.6 – 1.0	V

Anode inlet gas flow rate	0	
Cathode inlet gas flow rate	400	SCCM
Cathode gas composition	Air	
Cathode inlet gas temperature	1023 - 1173	K

Table. 5 Operation parameters for D_{ce} effect study in DC-SOFC

Parameter	**Value**	**Unit**
Operating potential	0.6 - 1	V
Distance between anode chamber and electrode, D_{ce}	59 - 2059	μm
Anode inlet gas flow rate	0	
Cathode inlet gas flow rate	400	SCCM
Cathode gas composition	Air	
Cathode inlet gas temperature	1073	K

List of Figures

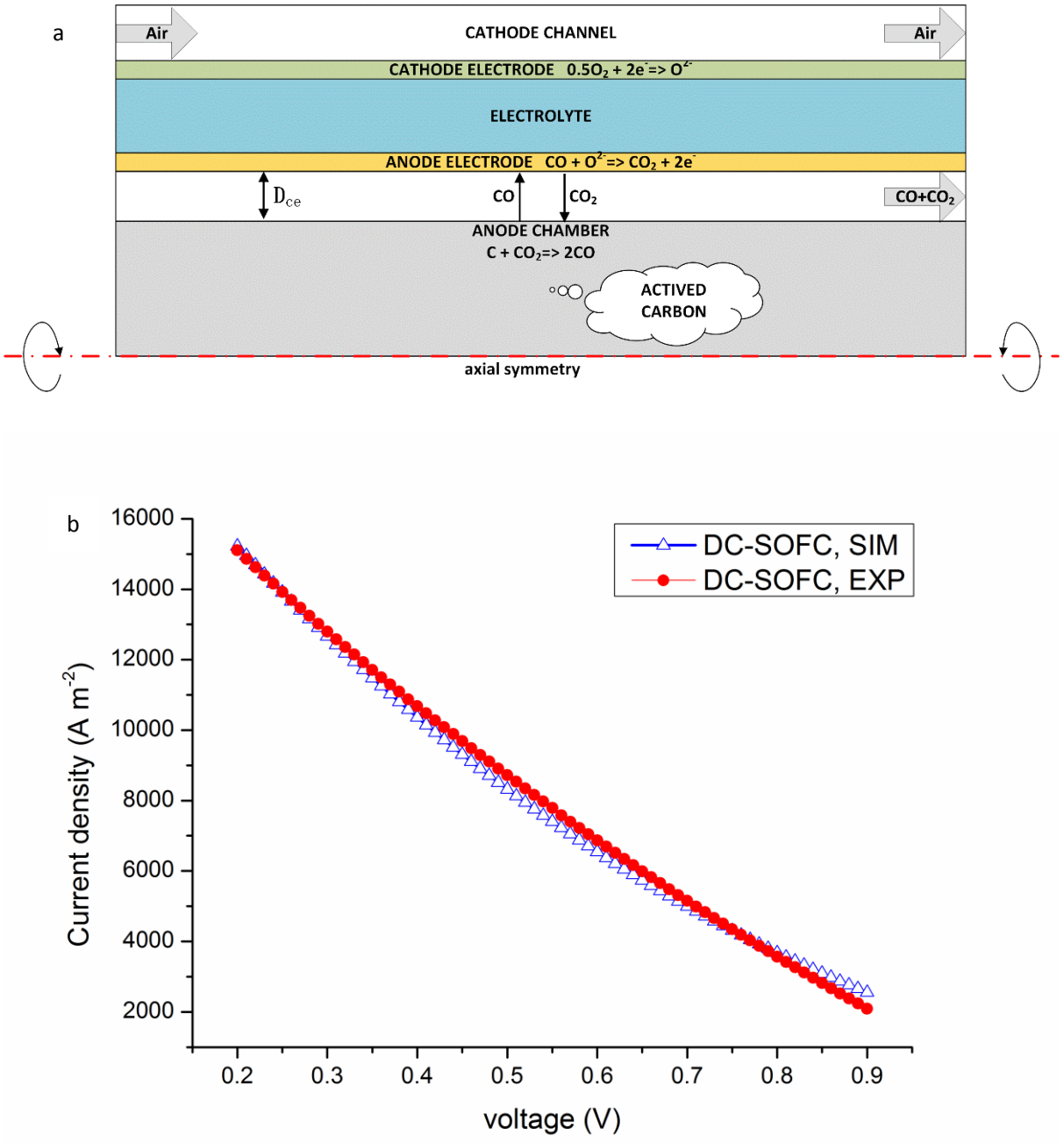

Fig.1. Schematic of the electrolyte supported DC-SOFC(a) and model validation for DC-SOFC.

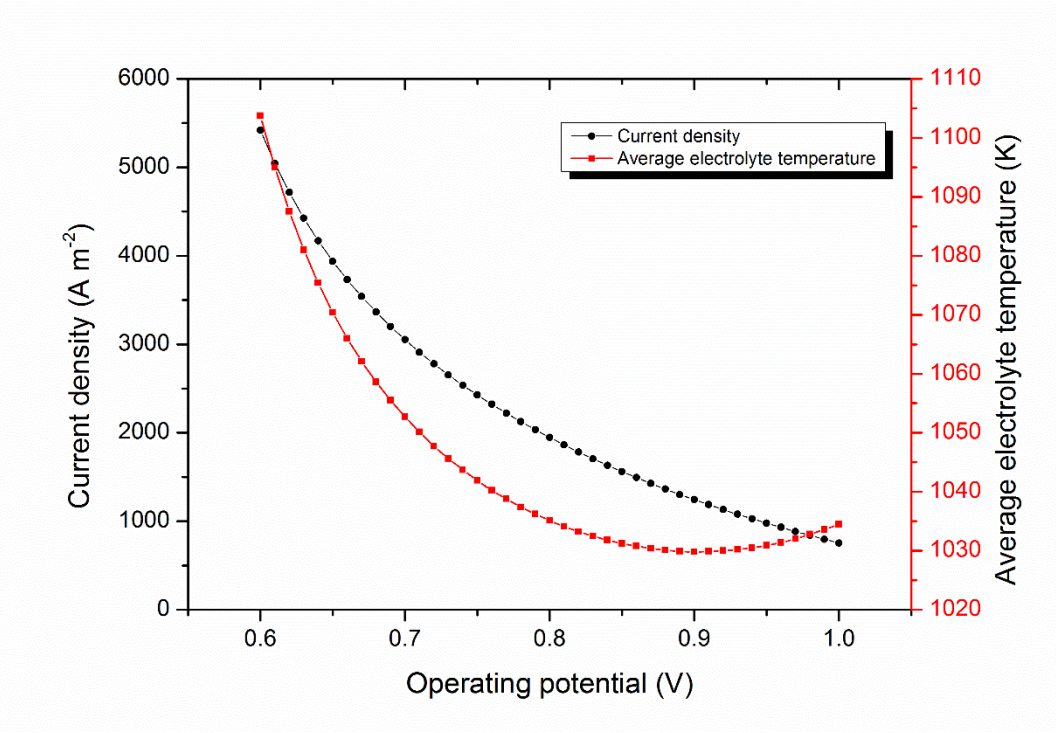

Fig. 2. Effect of operating potential on cell current density and temperature

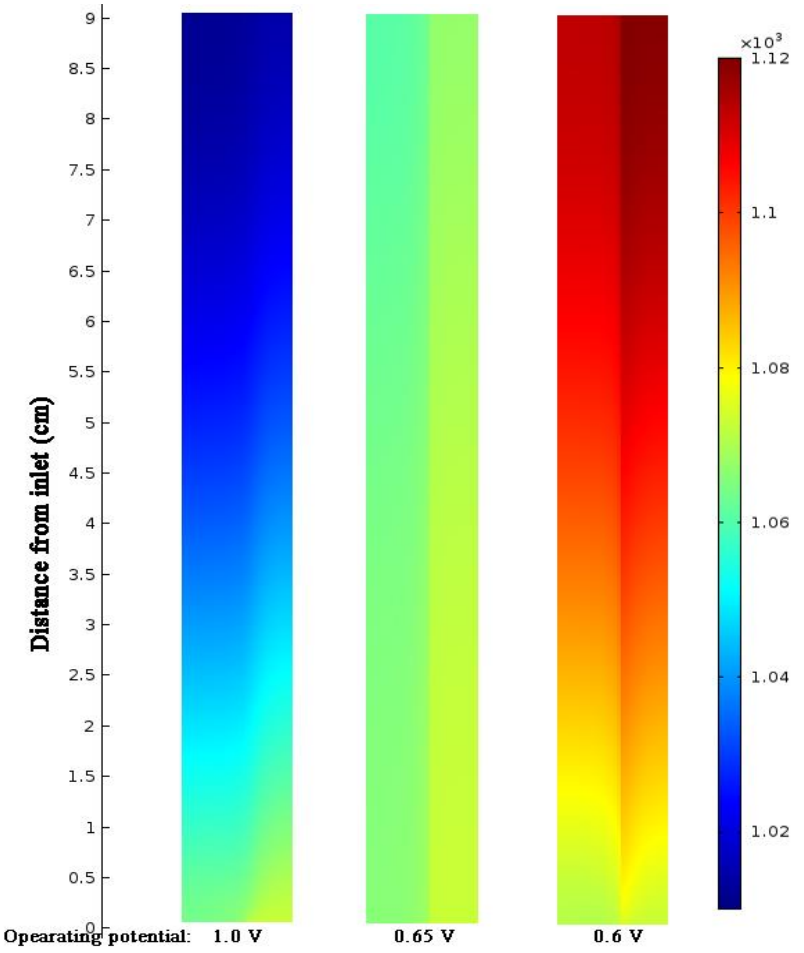

Fig. 3. Cell temperature distribution at 1.0 V, 0.65 V and 0.6 V operating potential.

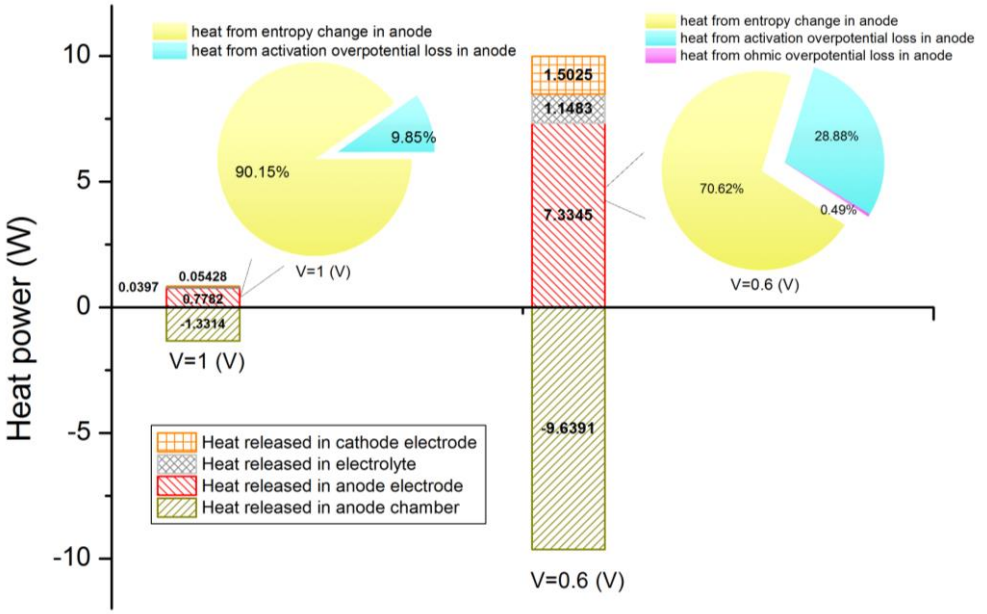

Fig. 4. Breakdown of heat power from different components in the cell.

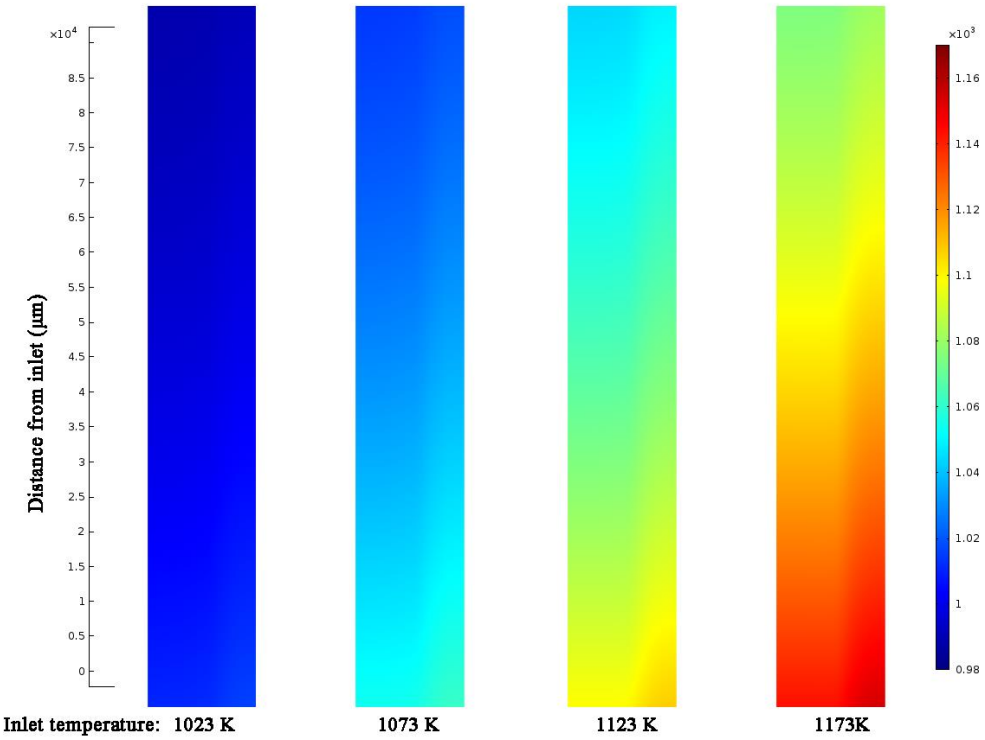

Fig. 5. Cathode inlet gas temperature effects on cell temperature distribution at 1.0 V

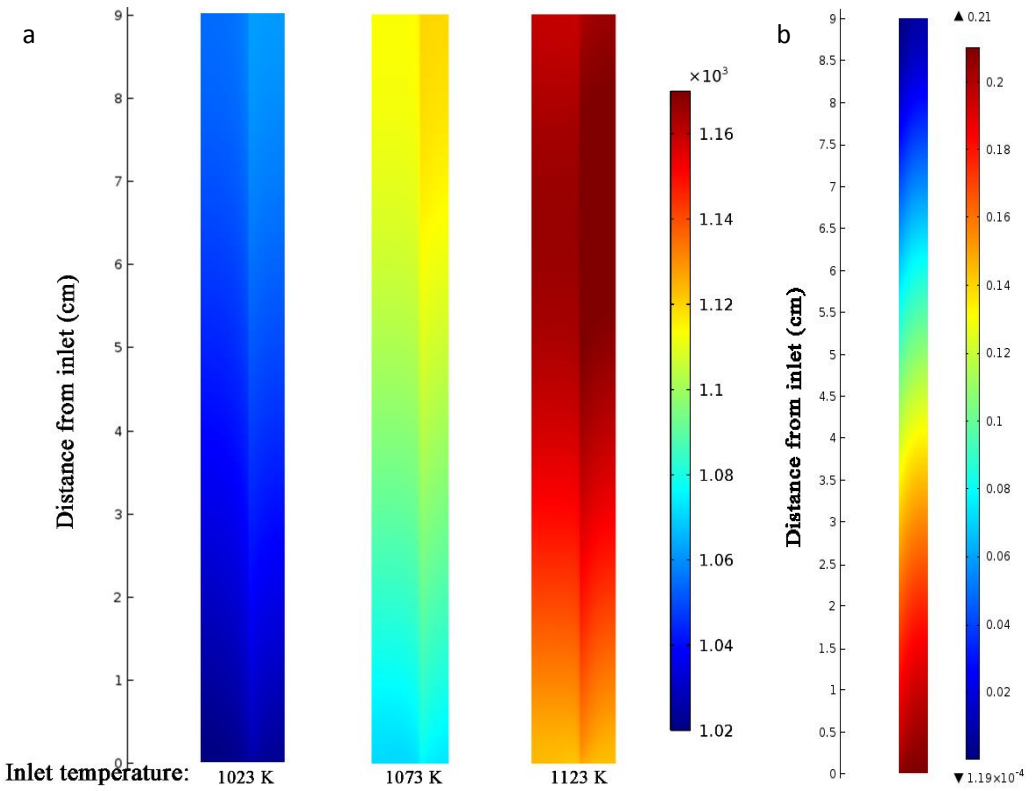

Fig. 6. Cathode inlet gas temperature effects on cell temperature distribution at 0.6 V operating potential (a) and cathode O_2 molar fraction (b) with 1123 K inlet gas temperature.

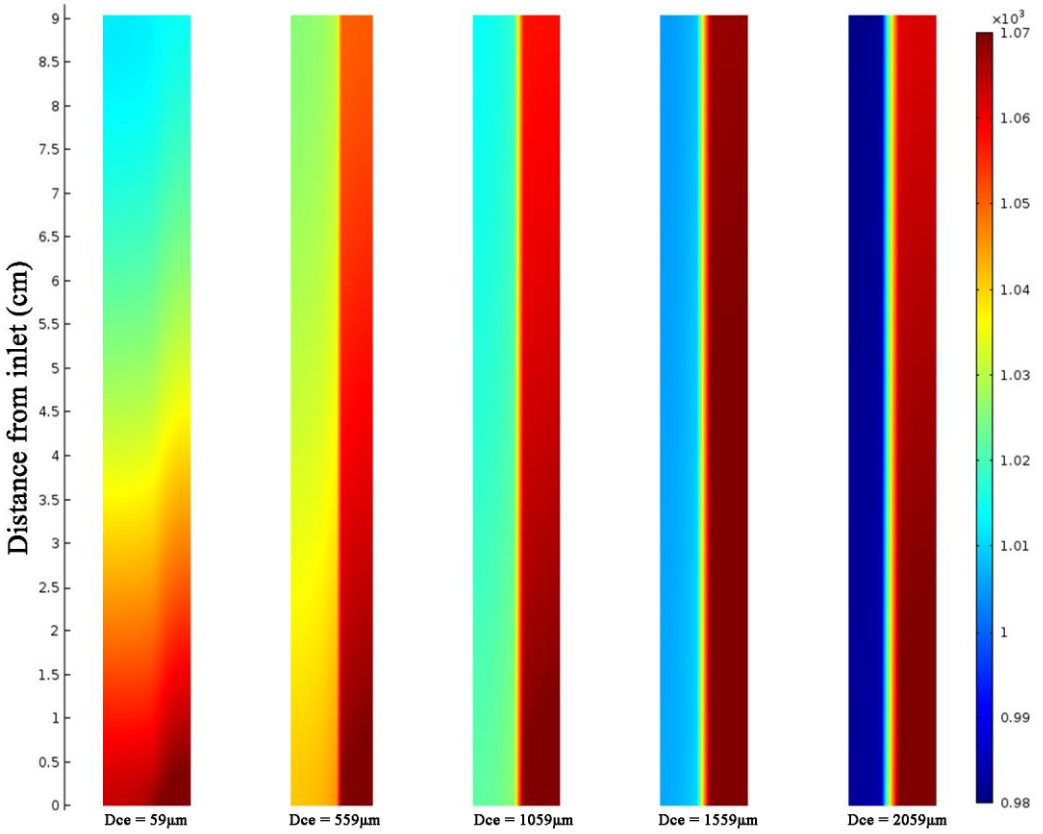

Fig. 7. Effects of Dce on the temperature distribution in the cell with 1073K cathode inlet gas temperature and 0.7 V operating potential

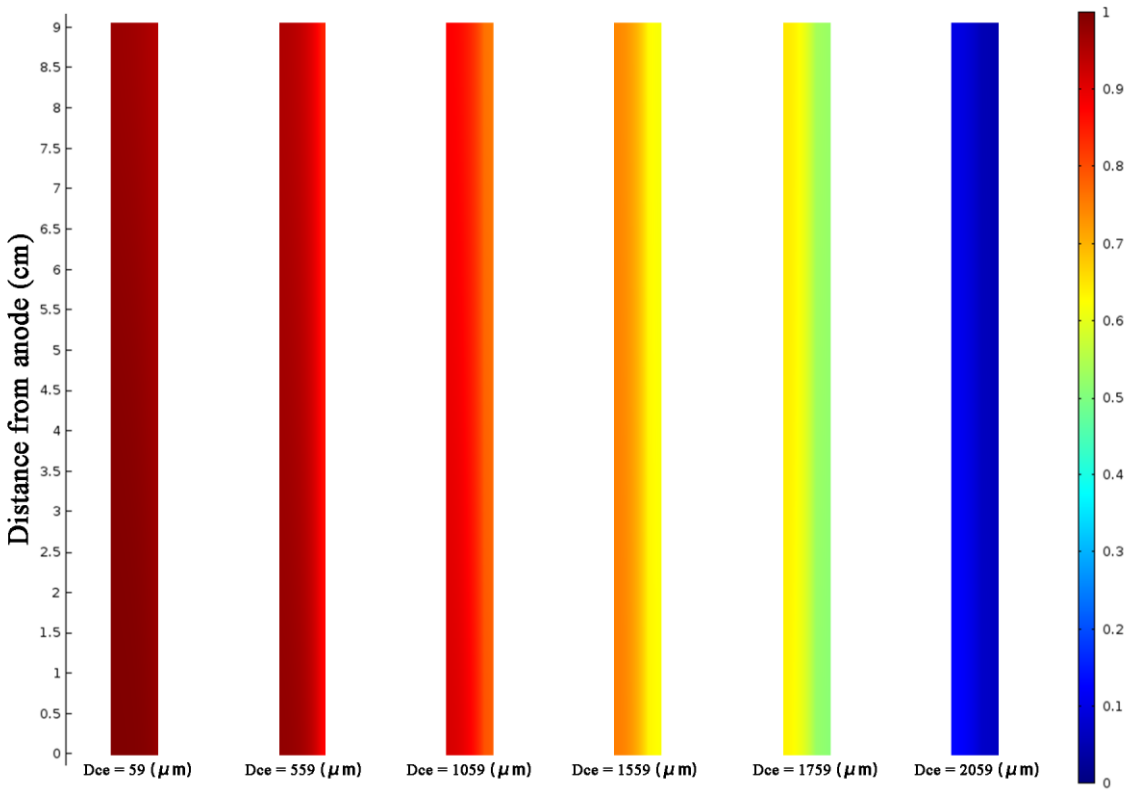

Fig. 8. Effects of Dce on the CO molar fraction distribution in the anode with 1073K cathode inlet gas temperature and 0.7 V operating potential